and product (Fig. 3). Protonation would be consistent with a structural role as an obligate hydrogen bond donor, rather than an acid-base catalyst (*22*). Presumably, proton transfer to and from the 2′-oxygen of nucleotide −1 is carried out by water. Investigation of the importance of the nucleobases of G8, A9, and A10 using abasic ribozyme constructs showed that individually, these purines contribute surprisingly little to catalytic rate enhancement (*23*), consistent with a role in binding or ribozyme architecture rather than general acid-base catalysis. Examination of the effect of adenosine base ionization on hairpin ribozyme activity with the use of nucleotide analog interference mapping (*24*) demonstrated that all pH-dependent interferences are due to structural destabilization of the RNA (*25*, *26*). Our transition state mimic and product structures (Fig. 3, B and C) suggest that N1 of A38 could have a perturbed pK_a, and this functional group could also play a role in protonating the leaving group during the cleavage reaction.

Pauling proposed in 1946 that enzymes could function by binding more tightly to the transition state than to the ground states, thus lowering the activation energy (*27*). The structural analysis presented here shows that the hairpin ribozyme has evolved to maximize its hydrogen bonding interactions with the trigonal bipyramidal transition state (Fig. 3) (*28*). For some protein enzymes, catalysis is known to result exclusively from binding energy (*29*). Like other RNA catalysts (*30*, *31*), the hairpin ribozyme also uses the binding energy of groups distant to the active site to accelerate its reaction: docking of stems A and B leads to a folding transition (*5*, *32*, *33*) that aligns the substrate within a rigid (*16*) active site. Precise positioning of substrate can effect large rate enhancements (*34*). Recent work on other catalytic RNAs, such as the ribosome (*35*), suggests that the combination of transition state stabilization and precise substrate positioning used by the hairpin ribozyme may be a catalytic strategy frequently used by RNA enzymes.

References and Notes

1. M. J. Fedor, *J. Mol. Biol.* **297**, 269 (2000).
2. A. Hampel, J. A. Cowan, *Chem. Biol.* **4**, 513 (1997).
3. K. J. Young, F. Gill, J. A. Grasby, *Nucleic Acids Res.* **25**, 3760 (1997).
4. S. Nesbitt, L. A. Hegg, M. J. Fedor, *Chem. Biol.* **4**, 619 (1997).
5. P. B. Rupert, A. R. Ferré-D'Amaré, *Nature* **410**, 780 (2001).
6. Materials and Methods are available as supporting online material on *Science* Online.
7. A. Wlodawer, M. Miller, L. Sjolin, *Proc. Natl. Acad. Sci. U.S.A.* **80**, 3628 (1983).
8. B. D. Wladkowski, L. A. Svensson, L. Sjolin, J. E. Ladner, G. L. Gilliland, *J. Am. Chem. Soc.* **120**, 5488 (1998).
9. R. N. Lindquist, J. L. Lynn Jr., G. E. Lienhard, *J. Am. Chem. Soc.* **95**, 8762 (1973).
10. M. Krauss, H. Basch, *J. Am. Chem. Soc.* **114**, 3630 (1992).
11. T. D. Veenstra, L. Lee, *Biophys. J.* **67**, 331 (1994).
12. H. Deng, J. W. Burgner, R. H. Callender, *J. Am. Chem. Soc.* **120**, 4717 (1998).
13. R. T. Raines, *Chem. Rev.* **98**, 1045 (1998).
14. J. M. Messmore, R. T. Raines, *J. Am. Chem. Soc.* **122**, 9911 (2000).
15. A. P. Massey, S. Th. Sigurdsson, in preparation.
16. All-atom superposition of the nucleobases of G8, A9, and A38 (31 atoms) gives root mean square (rms) differences of 0.32 Å and 0.31 Å for the precursor versus the transition state mimic, and the transition state mimic versus the product, respectively.
17. S. O. Shan, D. Herschlag, *Methods Enzymol.* **308**, 246 (1999).
18. W. Saenger, *Principles of Nucleic Acid Structure* (Springer-Verlag, New York, 1984), pp. 107–110.
19. A. T. Perrotta, I. Shih, M. D. Been, *Science* **286**, 123 (1999).
20. S. Nakano, D. M. Chadalavada, P. C. Bevilacqua, *Science* **287**, 1493 (2000).
21. R. Pinard *et al.*, *EMBO J.* **20**, 6434 (2001).
22. It has also been shown that deletion or methylation of the exocyclic amino group of G8 is deleterious for catalysis (*1*, *21*, *24*). This functional group hydrogen bonds to a nonbridging phosphate oxygen in both the precursor and the transition state (Figs. 1D, 2A, and 3).
23. L. L. Lebruska, I. I. Kuzmine, M. J. Fedor, *Chem. Biol.* **9**, 465 (2002).
24. S. P. Ryder, S. A. Strobel, *Nucleic Acids Res.* **30**, 1287 (2002).
25. S. P. Ryder *et al.*, *RNA* **7**, 1454 (2001).
26. When examined with the use of a stable RNA construct, the only adenosine functional group that interferes with ribozyme activity is the exocyclic amine of A38, and this interference is independent of pH (*25*). In both transition state and product, this amine donates a hydrogen bond to a nonbridging phosphate oxygen (Figs. 1D, 2A, and 3). In a destabilized construct, the exocyclic amine of A9 shows a pH-independent interference (*25*). This can be explained by the hydrogen bond it makes to the transition state (Figs. 1D and 3B).
27. L. Pauling, *Chem. Eng. News* **24**, 1375 (1946).
28. The ribozyme may also destabilize the precursor by desolvating the scissile phosphate and not saturating the partially buried anion with hydrogen bonds.
29. A. Fersht, *Structure and Mechanism in Protein Science* (Freeman and Co., New York, 1999), pp. 420–450.
30. G. J. Narlikar, V. Gopalakrishnan, T. S. McConnell, N. Usman, D. Herschlag, *Proc. Natl. Acad. Sci. U.S.A.* **92**, 3668 (1995).
31. K. J. Hertel, A. Peracchi, O. C. Uhlenbeck, D. Herschlag, *Proc. Natl. Acad. Sci. U.S.A.* **94**, 8497 (1997).
32. Z. Cai, I. J. Tinoco, *Biochemistry* **35**, 6026 (1996).
33. S. E. Butcher, F. H. Allain, J. Feigon, *Nature Struct. Biol.* **6**, 212 (1999).
34. M. I. Page, W. P. Jencks, *Proc. Natl. Acad. Sci. U.S.A.* **68**, 1678 (1971).
35. V. Ramakrishnan, *Cell* **108**, 557 (2002).
36. H. van Tol, J. M. Buzayan, P. A. Feldstein, F. Eckstein, G. Bruening, *Nucleic Acids. Res.* **18**, 1971 (1990).
37. A. T. Brünger *et al.*, *Acta Crystallogr.* **D54**, 905 (1998).

38. We thank the staff of beamlines 5.0.1 and 5.0.2 of the Advanced Light Source (ALS), Lawrence Berkeley National Laboratory, for data collection support; J. Bolduc, P. Heath, and B. Shen for crystallographic and computational support; P. Gafken for mass spectrometry; and J. Simon, B. Stoddard, and G. Varani for discussions. This work was supported by the NIH (grants GM63576 and RR15943 to A.R.F. and GM56947 to S.Th.S.). P.B.R. is a postdoctoral trainee of the Chromosome Metabolism and Cancer training grant from the National Cancer Institute to the Fred Hutchinson Cancer Research Center (FHCRC). Access to ALS beamlines 5.0.1 and 5.0.2 as part of the principal research consortium was funded by general support from the FHCRC. A.R.F. is a Rita Allen Foundation Scholar. Coordinates and structure factors have been deposited with the Protein Data Bank (accession codes 1M5K, 1M5O, 1M5V, and 1M5P for the methoxy, vanadate, all-RNA, and 5′-chloro structures, respectively).

Supporting Online Material

www.sciencemag.org/cgi/content/full/1076093/DC1
Materials and Methods
Figs. S1 to S4
Table S1

12 July 2002; accepted 16 September 2002
Published online 10 October 2002;
10.1126/science.1076093
Include this information when citing this paper.

Critical Roles of Activation-Induced Cytidine Deaminase in the Homeostasis of Gut Flora

Sidonia Fagarasan,[1,2]* Masamichi Muramatsu,[1]* Keiichiro Suzuki,[1] Hitoshi Nagaoka,[1] Hiroshi Hiai,[3] Tasuku Honjo[1]†

Activation-induced cytidine deaminase (AID) plays an essential role in class switch recombination (CSR) and somatic hypermutation (SHM) of immunoglobulin genes. We report here that deficiency in AID results in the development of hyperplasia of isolated lymphoid follicles (ILFs) associated with a 100-fold expansion of anaerobic flora in the small intestine. Reduction of bacterial flora by antibiotic treatment of $AID^{-/-}$ mice abolished ILF hyperplasia as well as the germinal center enlargement seen in secondary lymphoid tissues. Because an inability to switch to immunoglobulin A on its own does not lead to a similar phenotype, these results suggest that SHM of ILF B cells plays a critical role in regulating intestinal microflora.

Colonization of the intestine with microflora is essential for the normal development of humoral and cellular immune responses (*1*, *2*). Intestinal B cells are evolutionarily tailored largely for production of immunoglobulin A (IgA), which is transported across the epithelium into the gut lumen, where it serves as a first line of defense against viral and bacterial pathogens (*3*). It has been long recognized that a

large number of IgA plasma cells are derived from precursor B cells in the Peyer's patches (PP), which switch from IgM to IgA production, with the help of T cells, in the microenvironment provided by germinal centers (GC) (*4*). Besides PP, the presence of distinct organized lymphoid structures called isolated lymphoid follicles (ILFs) has been reported in the lamina propria (LP) of the intestine (*5*, *6*). Although a reciprocal relationship clearly exists between the intestinal flora and gut-associated lymphoid tissue (*1*), the mechanism by which gut-associated lymphoid tissue regulates the gut flora remains unclear.

AID is specifically expressed in GC B cells (*7*), and AID deficiency in mice and humans results in a defect in CSR and SHM (*8*, *9*). AID-deficient mice display a massive accumulation of intestinal IgM plasma cells (*10*) and enlarged GC in all lymphoid tissues, even in the absence of deliberate immunization (*8*). The presence of IgM plasma cells in the intestines of AID$^{-/-}$ mice was explained by the finding that LP B cells ordinarily switch preferentially to IgA and then differentiate to IgA plasma cells in situ, with the help of factors produced by LP stromal cells (*10*). In the absence of AID, this is prevented, which leads to IgM accumulation and PP enlargement.

We observed that AID$^{-/-}$ mice bred on a BALB/c or a C57BL/6 background developed not only unusually enlarged PP but also a striking number of protruding follicular structures on their small intestine (Fig. 1A). These structures were particularly pronounced on duodenal and jejunal segments of small intestines of AID$^{-/-}$ mice (fig. S1, A and B), and most protruding structures were located on the antemesenteric side. These were already visible by 5 weeks of age, and their number and size dramatically increased with age (Fig. 1, A and B). Immunohistochemical studies revealed that protruding structures of the LP had an architecture very similar to that of PP follicles (*11*). Thus, they were filled with IgM$^+$ B cells within a follicular dendritic cells (FDC) network (Fig. 1C, a and b), with T cells interspersed between B cells (Fig. 1C, c and d) and dendritic cells in a region that resembled the subepithelial dome of PP (Fig. 1C, e and f). The similarity in organization of these structures and ILFs (*6*) (Fig. 1C, a, c, and e) indicates that these represent significant hyperplasia of ILFs.

Enlargement of ILFs in BALB/c AID$^{-/-}$ mice was already detectable at day 9 after birth (Fig. 1D, a and b), and the size differences were even more pronounced by 21 days of age (Fig. 1D, c and d). Surprisingly, at these time points there were no obvious differences in size and structure of PP between AID$^{-/-}$, AID$^{+/-}$, and wild-type mice (Fig. 1D, g to j). Both LP and PP follicles of older AID$^{-/-}$ mice displayed considerable expansion of GC regions and reduced corona zones (Fig. 1D, f and l) compared with PP follicles in AID$^{+/-}$ mice (Fig. 1D, k). B cell accumulation was also found in mesenteric lymph nodes and spleens of older AID$^{-/-}$ mice (Fig. 2A), and B cells isolated from AID$^{-/-}$ mice appeared to be more activated than those from AID$^{+/-}$ mice housed under identical conditions (*12*). Consistent with this, more than half of ILF and PP B cells were B220$^+$PNA$^+$ cells involved in GC reactions (Fig. 2B). The absolute number of GC B cells in gut-associated lymphoid tissue as well as

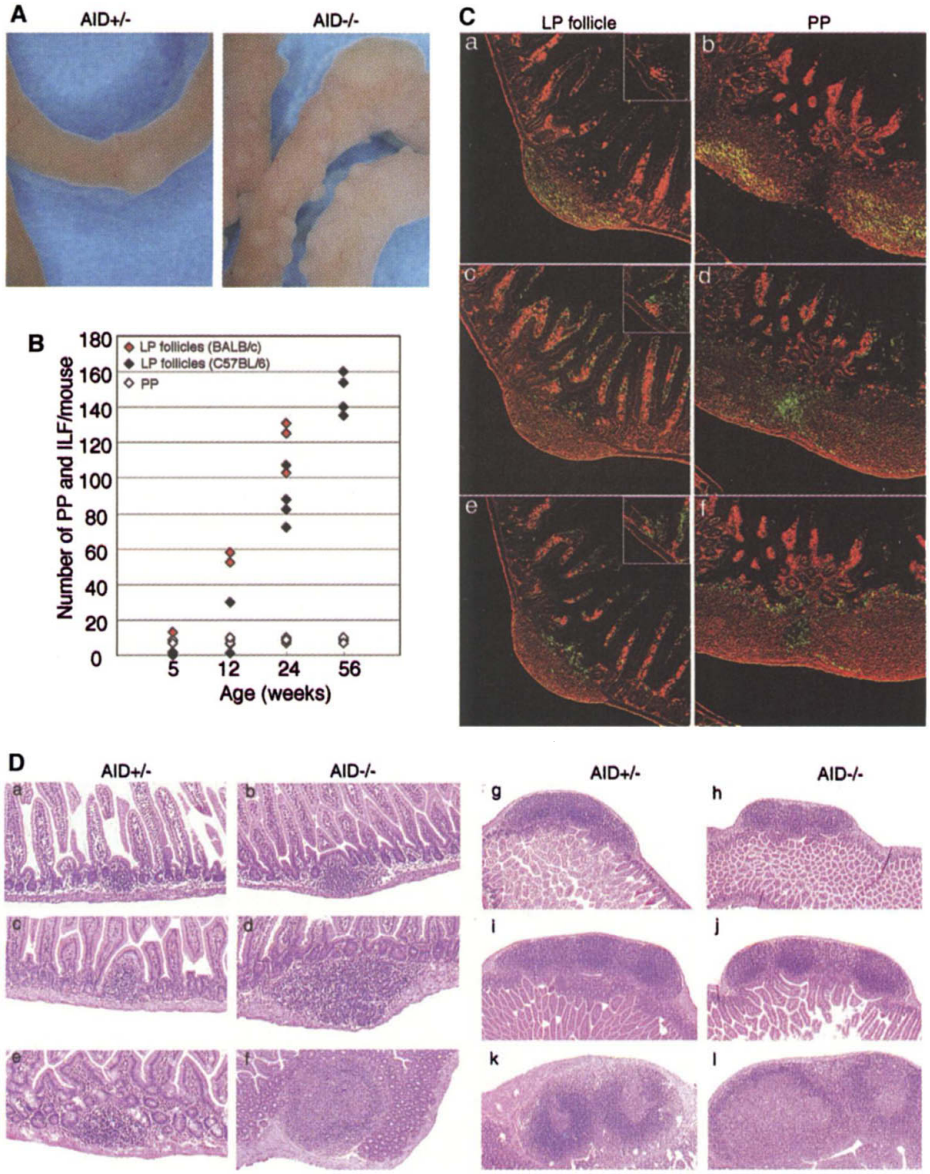

Fig. 1. Follicular hyperplasia in AID$^{-/-}$ small intestine. (**A**) Photograph of small intestine with PP (AID$^{+/-}$) and with PP and LP follicles (AID$^{-/-}$) of 20-week-old mice. (**B**) Number of PP and LP follicles (ILFs) in C57BL/6 mixed background and BALB/c AID$^{-/-}$ mice at the indicated ages. (**C**) Serial sections of LP follicles (a, c, and e) and PP (b, d, and f) from 20-week-old AID$^{-/-}$ mice stained for IgM (red) and CD21 (green) to detect FDC (a and b), CD3 (green) for T cells (c and d), and CD11c (green) for dendritic cells (e and f). Insets in (a, c, and e) represent sections of ILFs from AID$^{+/-}$ mice. Original magnification = ×10. (**D**) Hematoxylin and eosin section staining of LP follicles (a to f) and PP (g to l) from AID$^{+/-}$ (a, c, e, g, i, and k) and AID$^{-/-}$ (b, d, f, h, j, and l) mice. The ages of mice were 9 days (upper), 21 days (middle), and 20 weeks (lower). Original magnifications = ×10 (a to e) and ×4 (f to l).

[1]Department of Medical Chemistry, [3]Department of Pathology and Biology of Disease, Graduate School of Medicine, Kyoto University, Yoshida, Sakyo-ku, Kyoto 606-8501, Japan. [2]RIKEN Research Center for Allergy and Immunology, Tsurumi-ku, Yokohama, Kanagawa 230-0045, Japan.

*These authors contributed equally to this work.
†To whom correspondence should be addressed. E-mail: honjo@mfour.med.kyoto-u.ac.jp

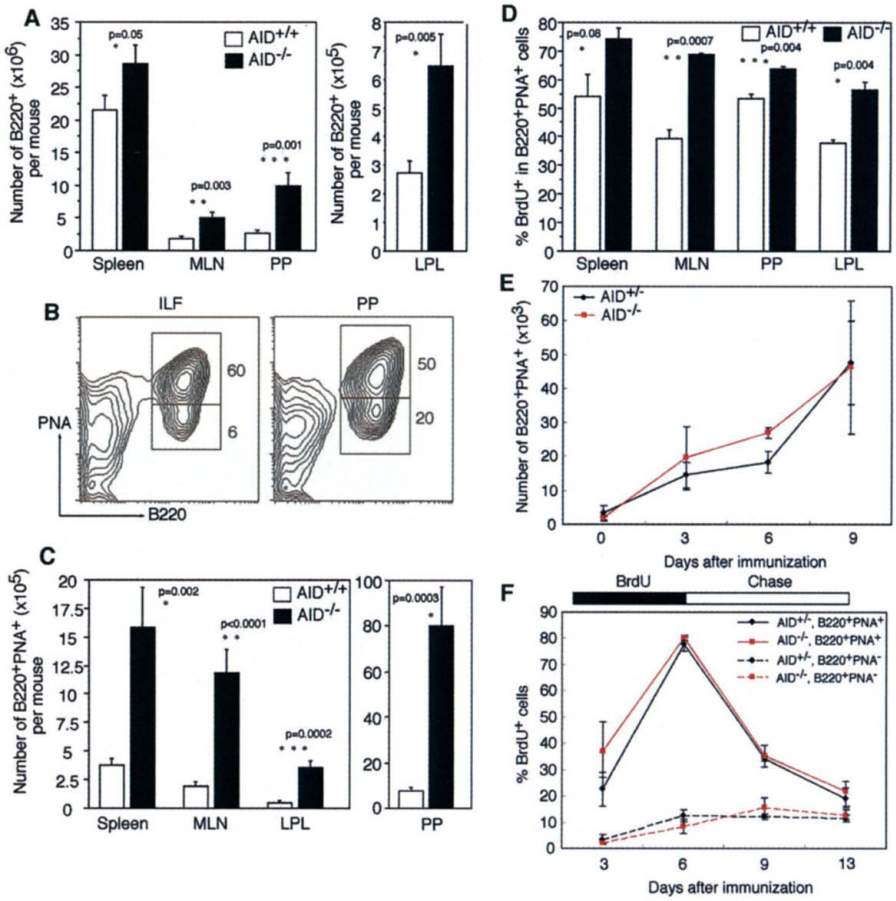

Fig. 2. Increased number of highly proliferating GC B cells in AID$^{-/-}$ mice. Total number of B220^{+} cells (**A**) and absolute number of GC B cells (**C**) in 20-week-old mice. Data represent mean ± SE (n = 12) for each mouse type. (**B**) Representative flow cytometric profiles of cells isolated from pooled protruding ILFs and all PP cells, stained for B220 and peanut agglutinin (PNA). Most B cells in ILFs and PP were B220^{+}PNA^{+}, involved in GC reactions. (**D**) Percentage of BrdU^{+} cells in B220^{+}PNA^{+} cells in AID$^{+/-}$ (white bars) and AID$^{-/-}$ (black bars) mice. Twenty-week-old mice received 0.6 mg of BrdU intraperitoneally every 12 hours for 6 days and were analyzed at day 7. Data represent mean ± SE (n = 3; unpaired Student's t test). (**E**) Total number of B220^{+}PNA^{+} cells in popliteal lymph nodes of 20-week-old AID$^{+/-}$ (black line) and AID$^{-/-}$ (red line) mice, before and after food pad immunization with NP-CGG/alum (mean ± SE; n = 3). (**F**) No significant differences in B cell proliferation and survival in de novo induced GC, as shown by percentages of labeled cells pulsed with BrdU for 6 days and then chased for another week (mean ± SE; n = 3). MLN = mesenteric lymph node, LPL = LP lymphocytes.

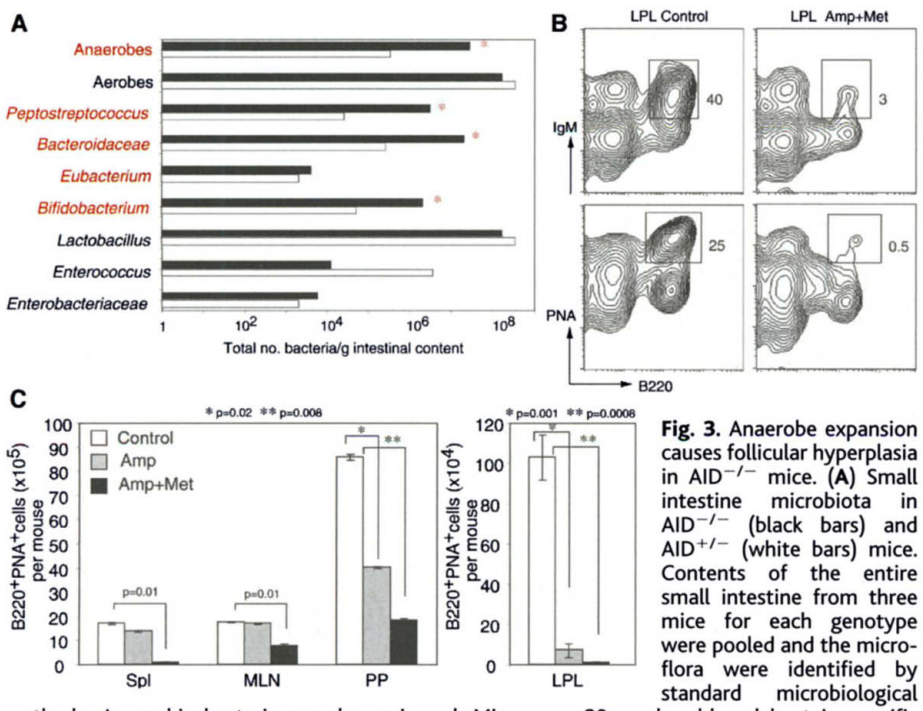

Fig. 3. Anaerobe expansion causes follicular hyperplasia in AID$^{-/-}$ mice. (**A**) Small intestine microbiota in AID$^{-/-}$ (black bars) and AID$^{+/-}$ (white bars) mice. Contents of the entire small intestine from three mice for each genotype were pooled and the microflora were identified by standard microbiological methods. Anaerobic bacteria are shown in red. Mice were 20 weeks old and kept in specific pathogen-free conditions. (**B**) Representative fluorescence-activated cell sorter (FACS) profiles of LP from 5-week-old nontreated and antibiotic-treated BALB/c AID$^{-/-}$ mice, stained for B220, IgM, and peanut agglutinin (PNA). Numbers indicate the percentages of lymphocytes in the gates. (**C**) Total number of B220^{+}PNA^{+} cells in 5-week-old control and antibiotic-treated BALB/c AID$^{-/-}$ mice. One set of mice (gray bars) received a mixture containing ampicillin, imipenem, and neomycin for 2 weeks. Another set of mice (black bars) received the same mixture for 1 week, followed by 1 week of metronidazole. Data are mean ± SE; n = 3; unpaired Student's t test; P values are shown.

in spleen was drastically increased in AID$^{-/-}$ mice compared with the number in control mice (Fig. 2C).

We found that more B220^{+}PNA^{+} cells incorporated bromodeoxyuridine (BrdU) in AID$^{-/-}$ than in AID$^{+/-}$ mice (Fig. 2D). To examine whether the enhanced proliferation of GC B cells in AID$^{-/-}$ mice was due to intrinsic defects in AID-deficient B cells, we studied the kinetics of de novo GC formation by immunization. We chose popliteal lymph nodes because of a very small number of GC in nonimmunized mice (Fig. 2E). The total numbers of B220^{+}PNA^{+} B cells in popliteal lymph nodes of both AID$^{-/-}$ and AID$^{+/-}$ mice gradually increased at days 3, 6, and 9 after immunization. Therefore, we assumed that the large majority of GC (a 10-fold increase by day 9) was induced de novo and had developed in a synchronized manner (Fig. 2E). We found no significant differences of B cell proliferation and survival in induced GC, as determined by BrdU labeling in a pulse-chase experiment (Fig. 2F), in agreement with our in vitro data (*8*). Thus, the increased uptake of BrdU in nonmanipulated AID-deficient mice is likely due to an intense antigenic stimulation with constant induction of GC formation.

We next examined whether gut flora might be disregulated in the absence of IgA switching and/or SHM. When 20-week-old

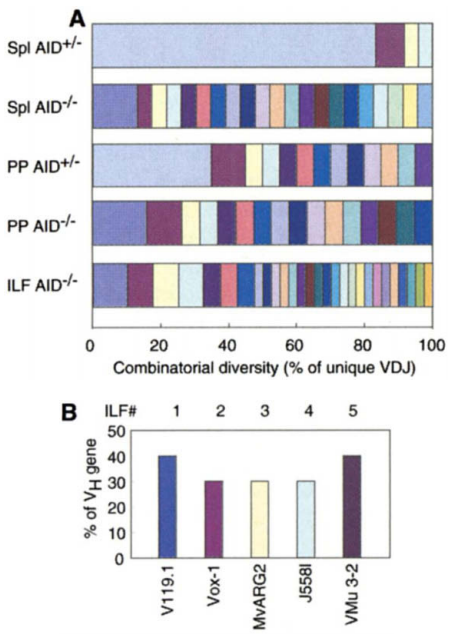

Fig. 4. Repertoire diversity of ILF B cells. **(A)** Combinatorial diversity in IgM B cells isolated from four protruding ILFs, all PP (n = 8) and spleen (Spl) from 56-week-old $AID^{-/-}$ and $AID^{+/-}$ mice, as calculated by the frequency of transcripts of a given in-frame VDJ rearrangement. Two mice were analyzed for each genotype. Each color represents a unique VDJ rearrangement. **(B)** Different predominant V_H genes among B cells isolated from five individual ILFs isolated from duodenal, jejunal, and ileal segments of 56-week-old $AID^{-/-}$ mice, shown as frequency of the indicated genes in sequenced clones.

mice housed under specific pathogen-free conditions were analyzed, a 100-fold increase in the number of anaerobic bacteria was apparent in the small intestines of $AID^{-/-}$ mice (Fig. 3A). In contrast, the small intestine microbiota of age-matched $AID^{+/-}$ mice were dominated by aerobic bacteria and only 0.1% of microflora were composed of anaerobes (Fig. 3A). The total number of bacteria in the small intestine was comparable in $AID^{-/-}$ and $AID^{+/-}$ mice (1.9×10^8 and 3.3×10^8 bacteria per g of intestinal contents, respectively). However, unlike normal mice, which contain anaerobes predominantly in cecal fluid and the large intestine (*1*), the anaerobic expansion observed in $AID^{-/-}$ mice was generalized throughout the small intestine (fig. S1C). The complexity of microbiota and the total numbers of bacteria found in upper and middle segments of the small intestine of $AID^{-/-}$ mice were very high, although less than in cecum, and comparable with that of lower segments (fig. S1D). No significant changes could be detected in the flora of the large intestine of $AID^{-/-}$ mice (*12*).

To determine the potential involvement of gut microbiota in the induction of follicular hypertrophy in LP of $AID^{-/-}$ mice, we decreased the intestinal flora by oral administration of large-spectrum antibiotics, which covered both aerobic and anaerobic bacteria (*11*). After 2 weeks of treatment, protruding follicles were either absent or very strongly reduced along the small intestine. This corresponded with a decrease in the number of anaerobes in the small intestine below the limits of detection (*12*). This was also reflected in a dramatic reduction of $B220^+PNA^+$ GC B cells and $B220^+IgM^+$ GC B cells, especially in the LP of treated $AID^{-/-}$ mice (Fig. 3, B and C). Strikingly, antibiotic treatment (metronidazole) directed against anaerobic bacteria decreased B cell activation in all lymphoid tissues, as shown by a marked reduction in the number of GC B cells (Fig. 3C), thus emphasizing the impact of exacerbated numbers of intestinal anaerobes on the nonmucosal immune system.

To confirm that the massive expansion of B cells in $AID^{-/-}$ mice resulted from antigenic stimulation, we sequenced and compared the repertoire of the variable region of immunoglobulin heavy-chain (V_H) genes from IgM B cells in older $AID^{-/-}$ and $AID^{+/-}$ mice. The repertoire of spleen or lymph node B cells in aged mice was oligoclonal in the absence of external stimulation but became polyclonal after in vitro lipopolysaccharide (LPS) stimulation (*13*). We found that, in $AID^{-/-}$ mice over 50 weeks of age, the repertoire of B cells isolated from hyperplastic follicles was diverse, consisting of many kinds of V_H genes and their combinatorial VDJ sequences (Fig. 4A). By comparison, the repertoire of B cells in PP of older $AID^{-/-}$ mice was less complex (24 VDJ per 38 clones sequenced) than in LP follicles (52 VDJ per 60 clones) (Fig. 4A) and was comparable to the diversity of PP B cells from age-matched $AID^{+/-}$ mice (30 VDJ per 40 clones) (Fig. 4A). The repertoire of B cells in spleens of $AID^{-/-}$ mice was also diverse, contrasting with an oligoclonal expansion of spleen B cells in $AID^{+/-}$ mice (Fig. 4A). Interestingly, the representation of the predominant V_H gene was different in each individual follicle (Fig. 4B), suggesting that selection and expansion of B cells was likely to have taken place in situ, possibly depending on the prevailing antigenic diversity of local bacteria.

The evidence presented here supports the proposal that ILF B cells play a major role in maintaining gut homeostasis. In the absence of both CSR and SHM, anaerobic bacteria were able to expand and induced hyperplasia of ILF and overstimulation of the nonmucosal immune system and enormous expansion of GC B cells. Importantly, IgA-deficient mice do not develop ILF hyperplasia in the small intestine (*14*) despite a similar accumulation of IgM in place of IgA and well-developed PP with enlarged GC in these animals (*15*). Because SHM is completely abrogated in the absence of AID expression (*8*) but not in $IgA^{-/-}$ mice, the significantly more severe phenotype in $AID^{-/-}$ mice indicates the importance of SHM in the gut. In this respect, SHM would enhance the diversity of local B cells, and this may be a critical feature for homeostatic control of gut bacteria.

The follicular phenotype we described for $AID^{-/-}$ mice resembles nodular lymphoid hyperplasia, a lymphoproliferative disorder associated with common variable immunodeficiency syndrome (*16*). Strikingly, patients with common variable immunodeficiency syndrome manifesting nodular lymphoid hyperplasia have not only extremely low levels of IgA, or IgG, but also a dramatic reduction in SHM of IgV genes (*17*). Although the cause of the development of follicular hyperplasia in humans remains unknown, it was suggested to occur as a result of local immune responses to the gut antigens (*18*). We showed that, at least in mice, this extreme hyperplasia of ILF was due to a disregulation of the commensal bacteria and that appropriate antibiotic treatment could abolish this phenotype. Our analysis of $AID^{-/-}$ mice thus opens new perspectives for clinical studies on mucosal immune diseases.

References and Notes

1. J. J. Cebra, *Am. J. Clin. Nutr.* **69**, 1046S (1999).
2. L. V. Hooper, J. I. Gordon, *Science* **292**, 1115 (2001).
3. P. Brandtzaeg *et al.*, *Immunol. Today* **20**, 141 (1999).
4. J. J. Cebra, K. E. Shroff, in *Handbook of Mucosal Immunology*, P. Ogra *et al.*, Eds. (Academic Press, San Diego, 1994), pp. 151–157.
5. M. Moghaddami, A. Cummins, G. Mayrhofer, *Gastroenterology* **115**, 1414 (1998).
6. H. Hamada *et al.*, *J. Immunol.* **168**, 57 (2002).
7. M. Muramatsu *et al.*, *J. Biol. Chem.* **274**, 18470 (1999).
8. M. Muramatsu *et al.*, *Cell* **102**, 553 (2000).
9. P. Revy *et al.*, *Cell* **102**, 565 (2000).
10. S. Fagarasan, K. Kinoshita, M. Muramatsu, K. Ikuta, T. Honjo, *Nature* **413**, 639 (2001).
11. Materials and methods are available on *Science* Online.
12. S. Fagarasan, unpublished data.
13. J. LeMaoult *et al.*, *J. Immunol.* **159**, 3866 (1997).
14. D. Metzger, personal communication.
15. G. R. Harriman *et al.*, *J. Immunol.* **162**, 2521 (1999).
16. C. Bastlein *et al.*, *Endoscopy* **20**, 272 (1988).
17. Y. Levy *et al.*, *Proc. Natl. Acad. Sci. U.S.A.* **95**, 13135 (1998).
18. R. W. Burt, R. F. Jacoby, in *Textbook of Gastroenterology*, T. Yamada *et al.*, Eds. (Lippincott Williams & Wilkins, Philadelphia, 1999), vol. II, pp. 1995–2022.
19. We are grateful to D. Metzger and members of T.H.'s laboratory for helpful discussions. Supported in part by a Center of Excellence Grant from the Ministry of Education, Science, Sports and Culture of Japan.

Supporting Online Material

www.sciencemag.org/cgi/content/full/298/5597/1424/DC1
Materials and Methods
Fig. S1

14 August 2002; accepted 24 September 2002